Modelling of ducted noise sources in the proximity of acoustic liners

Sergi Palleja-Cabre[1], Brian J. Tester, R. Jeremy Astley

Institute of Sound and Vibration Research, University of Southampton, Southampton, SO17 1BJ, UK

Abstract

This paper focuses on modelling and predicting the acoustic field generated by ducted point sources in close proximity to an acoustic liner. Two analytical models are presented. The first model comprises a point monopole or dipole source in an infinite lined duct based on an existing Green's function. The predictions are compared with classic solutions for a source over an infinite lined plane and with a high frequency asymptotic duct approximation. The second model extends the Green's function to include a liner section of finite length connected to hard-wall extensions by using mode-matching techniques. The new model features the inclusion of point sources in the vicinity of an impedance discontinuity. The accuracy of this model is demonstrated by comparison with reference FE solutions. Both models indicate a significant impact of the source proximity to the liner surface in the source power output. These models offer insight on the source modification effects beyond the conventional approach in the design of liners solely based on acoustic absorption.

Keywords: Source proximity liners, noise reduction, mode-matching, duct acoustics

[1]Corresponding author. E-mail address: S.Palleja-Cabre@soton.ac.uk

1. Introduction

Ducted fans are widely used in industry across different sectors including aerospace, automotive and a multitude of heating, cooling and ventilation systems at various scales. Compliance with environmental noise regulations has influenced manufacturers to treat acoustic pollution as one of the driving factors in the design of their products. Acoustic liners have traditionally been used in ducted systems to attenuate noise. This is especially the case in the aerospace industry where liners are an essential treatment for turbofan noise reduction and are universally installed in the intake and bypass ducts of modern commercial aircraft engines. Typical designs are formed by perforated or porous face sheets supported by one or multiple layers of honeycomb structure. These so-called Single-Degree-Of-Freedom (SDOF) and Multiple-Degree-Of-Freedom (MDOF) liners are generally designed to attenuate tonal and broadband noise over a prescribed range of frequencies to minimize the certification noise levels. The design of innovative liner configurations, the modelling of the physics involved in their absorption of noise and the measurement of their acoustic behaviour have been the subject of research for many years [1, 2, 3].

The authors of the current article are motivated by an interest in Fan Proximity Liners (FPL). These are acoustic treatments installed in the duct casing in the immediate proximity of the fan rotor. They comprise the fancase liner immediately upstream of the fan, Over-Tip-Rotor (OTR) liners proposed for the fan stage itself and interstage liners between the fan and outlet guide vanes. OTR liners have been in the spotlight following recent experimental evaluation [4, 5, 6, 7]. Published data [5] indicate that OTR liners not only attenuate noise by conventional absorption of acoustic energy within the liner, but also by modifying the strength of the source due to back reaction pressure effects, which arise from the very close proximity of the rotor tip sources to the lined surface.

The acoustic power generated by a point source in the presence of an acoustically treated surface is different from that in the free-field or in the presence of a

hard-wall. Analytical models have been developed in the literature to compute the acoustic field generated by a point source over an infinite lined plane. These include the works of Thomasson [8] and Levine [9] for a monopole in the absence of a background flow and 2D solutions of Brambley and Gabard [10] for a line source with uniform flow. For ducted applications, Green's functions have been published for infinite circular hollow ducts with uniform flow by Tester [11], Zorumski [12] and Alonso [13], and generalised for annular ducts by Rienstra and Tester [14]. Despite the availability of these analytical solutions, the implications on the noise radiation of point sources located acoustically close to a lined wall have not been fully explored in the past.

This work focuses on modelling and predicting the acoustic power radiated by point sources in close proximity to acoustic liners to improve understanding of the source modification effects observed in published tests of OTR liners [4, 5, 6, 7], and the extent to which they affect overall attenuation. A preliminary report of the current study was presented in [15]. Uniform axial mean flow has been assumed throughout the formulation presented here, a reasonable approximation for fancase liners and OTR liners. The latter are generally more challenging since the fan tip sources are then immediately adjacent to the liner surface. Linear propagation is assumed in the current study and sources are represented as point or distributed stationary volume velocity monopoles and oscillating force dipoles. The main assumptions of the proposed model for the prediction of the noise generation of FPLs are summarised in Table 1.

Table 1: Main assumptions of the analytical FPL liner prediction model.

Geometry	Axially segmented hollow circular duct
Propagation	Linear
Mean flow	Uniform axial (subsonic)
Impedance	Locally reacting, Ingard-Myers boundary condition
Source	Point and distributed stationary monopoles and dipoles

The propagation model which is based on Green's functions for infinite hard

or lined cylindrical hollow ducts containing uniform mean flow is described in Section 2. The effect of source proximity to the lined wall on the source power output is discussed in Section 3 for an infinite lined duct. The prediction model is modified in Section 4 to include a lined section of finite length connected to infinite hard-wall extensions. The fan sources are placed either immediately downstream of the lined section, to simulate a fancase liner, or within the lined section, to simulate an OTR liner. Mode-matching is used to connect the lined segment to the hard-walled extensions. Challenges arise when the source is close to the matching interfaces and this is also discussed in Section 4. Cross-verification of key aspects of the Green's function models against reference FEM solutions is also presented.

While the current work is motivated by the authors' interest in fan proximity liners for turbofan engines, the methods presented here offer insight into a broader class of problems in which sources are located close to lined surfaces in ducted systems. In the results presented here the critical parameters (duct dimensions, frequency, Mach number, etc.) are chosen however to demonstrate the performance of such configurations in turbofan applications.

2. Analytical model for an infinite lined duct (Green/INF)

2.1. A Green's function for an infinite anechoic duct

Consider solutions for the steady time harmonic acoustic field generated by an acoustic source, or distribution of sources, in a lined circular duct with uniform axial mean flow. The problem is sketched in Fig. 1. In all analysis which follows non-dimensional variables will be used; distances are normalised by the duct radius a, time by a/c_0, frequency by c_0/a, pressure by $\rho_0 c_0^2$, and particle velocity by c_0, where ρ_0 is the fluid density and c_0 is the speed of sound. The intensity is normalised by $\rho_0 c_0^3$ and the power by $\rho_0 c_0^3 a^2$. The axial mean flow velocity U_0 is normalised by c_0 to give a mean flow Mach number, $M = U_0/c_0$. The $\mathrm{e}^{\mathrm{j}\omega t}$ convention has been used to define time-harmonic variables.

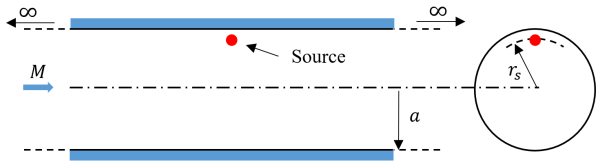

Figure 1: Lateral and cross-section of the infinite circular duct problem.

A customised Green's function $G(\boldsymbol{x}|\boldsymbol{y})$ for the above problem, where $\boldsymbol{x} = (x, r, \theta)$ denotes a field point and $\boldsymbol{y} = (x_s, r_s, \theta_s)$ denotes a source location, is defined to be a solution of the inhomogeneous convected Helmholtz pressure equation

$$\frac{\partial^2 G}{\partial x^2} + \frac{\partial^2 G}{\partial r^2} + \frac{1}{r}\frac{\partial G}{\partial r} + \frac{1}{r^2}\frac{\partial^2 G}{\partial \theta^2} - \left(\mathrm{j}\omega + M\frac{\partial}{\partial x}\right)^2 G = \delta(\mathbf{x} - \mathbf{y}) \quad , \qquad (1)$$

which also satisfies the Ingard-Myers impedance boundary condition at the wall:

$$\left(\mathrm{j}\omega + M\frac{\partial}{\partial x}\right)^2 G + \mathrm{j}\omega Z \frac{\partial G}{\partial r} = 0 \quad \text{at} \quad r = 1 \quad . \qquad (2)$$

The Green's function is unique if anechoic conditions exist as $x \to \pm\infty$.

An analytic Green's function for this problem was proposed by Tester et al. [16, 11]; extending a previous formulation for a 2D lined duct with uniform mean flow [17]. An equivalent formulation was independently obtained by Zorumski [12], although some of the expressions were not given explicitly. Alonso et al. [18, 19, 13] derived a Green's function by solving a linear system of equations based on a modal expansion of the solution and enforcing continuity of the solution at the source plane.

The analytic Green's function adopted here is the version derived by Rienstra and Tester [14], expressed as a sum of non-orthogonal modes obtained by representing the solution as a Fourier integral evaluated as a summation over the residues. The formulation is explicit and agrees with the Green's function of Alonso et al. [13] when a sufficient number of modes in both solutions are considered.

The Green's function is expressed as a sum of non-orthogonal modes

$$G(\boldsymbol{x}|\boldsymbol{y}) = \sum_{m=-\infty}^{\infty} \mathrm{e}^{-jm(\theta-\theta_s)} G_m(r, x, r_s, x_s) \quad , \tag{3}$$

where

$$G_m(r, x, r_s, x_s) = -\frac{1}{2\pi \mathrm{j}} \sum_{n=1}^{\infty} \frac{J_m(\alpha_{mn}^{\pm} r) J_m(\alpha_{mn}^{\pm} r_s)}{Q_{mn}^{\pm} J_m(\alpha_{mn}^{\pm})^2} \mathrm{e}^{-\mathrm{j}\kappa_{mn}^{\pm}(x-x_s)} \quad , \tag{4}$$

with

$$Q_{mn}^{\pm} = \pm \left[(\kappa_{mn}^{\pm} + \Omega_{mn}^{\pm} M) \left(1 - \frac{m^2}{\alpha_{mn}^{\pm 2}} - \frac{\Omega_{mn}^{\pm 4}}{(\omega \alpha_{mn}^{\pm} Z)^2} \right) - \frac{2jM\Omega_{mn}^{\pm}}{\omega Z} \right] \quad , \tag{5}$$

and where α_{mn} and κ_{mn} are the radial and axial eigenvalue pairs of azimuthal order m and radial order n that satisfy the eigenvalue equation

$$\mathrm{j}\Omega^2 J_m(\alpha) + \omega \alpha Z J_m'(\alpha) = 0 \quad , \tag{6}$$

where $\Omega = \omega - \kappa M$ satisfies the dispersion relation

$$\Omega^2 = \alpha^2 + \kappa^2 \quad . \tag{7}$$

$Q_{mn}^{\pm}$, $\alpha_{mn}^{\pm}$ and $\kappa_{mn}^{\pm}$ are used in Eq. (4-5) for the right-running (+) and left-running modes (-), in the regions $x > x_s$ and $x < x_s$ respectively. The solutions of the eigenvalue equation have been obtained in the current study by using a routine developed by Rienstra, in which the eigenvalue equation can be expressed in the form of an ODE and integrated numerically as an initial value problem. More details of the eigensolver and the analogous expressions for an annular section can be found in [14].

2.2. Monopole and dipole point sources

The sound field in the duct, $p(\boldsymbol{x}, \omega)$, due to distributed volume velocity monopole sources of complex amplitude $q(\boldsymbol{x}, \omega)$ and oscillating forces of amplitude $f(\boldsymbol{x}, \omega)$ is a solution of Eq. (1) and the boundary condition in Eq. (2) with the delta function on the RHS of Eq. (1) replaced by the source distribution

$$\mathrm{Q}(\boldsymbol{x}, \omega) = -\left(\mathrm{j}\omega + M \frac{\partial}{\partial x} \right) q(\boldsymbol{x}, \omega) + \boldsymbol{\nabla} \cdot \boldsymbol{f}(\boldsymbol{x}, \omega) \quad . \tag{8}$$

The general solution obtained by applying the Green's function described in Section 2.1 (Eq. (3-7)) is therefore

$$p(\boldsymbol{x},\omega) = \int_{V_s} G(\boldsymbol{x},\boldsymbol{y})\mathrm{Q}(\boldsymbol{y},\omega)dV_s(\boldsymbol{y}) \quad , \tag{9}$$

where V_s is a volume which encloses the distributed source and $\mathrm{Q}(\boldsymbol{y},\omega) = 0$ on the boundary surface of V_s. Substitution of Eq. (8) into Eq. (9) and use of integration by parts and the divergence theorem then gives

$$p(\boldsymbol{x},\omega) = \int_{V_s} \left[-\mathrm{j}\omega q(\boldsymbol{y},\omega)G(\boldsymbol{x},\boldsymbol{y}) + q(\boldsymbol{y},\omega)M\frac{\partial}{\partial x_s}G(\boldsymbol{x},\boldsymbol{y}) + \boldsymbol{f}(\boldsymbol{y},\omega)\cdot\boldsymbol{\nabla}_{\boldsymbol{y}}G(\boldsymbol{x},\boldsymbol{y}) \right] dV_s(\boldsymbol{y}) \quad . \tag{10}$$

The expression for a volume velocity monopole can be readily obtained by substitution of

$$q(\boldsymbol{y},\omega) = q_0\delta(\boldsymbol{x}-\boldsymbol{y}) \quad , \tag{11}$$

where q_0 is the monopole strength, into Eq. (10) and setting $\boldsymbol{f}(\boldsymbol{y},\omega) = 0$ to give

$$p(\boldsymbol{x},\omega) = q_0 \sum_{m=-\infty}^{\infty} \mathrm{e}^{-\mathrm{j}m(\theta-\theta_s)} \left(\frac{1}{2\pi} \sum_{n=1}^{\infty} \Omega_{mn}^{\pm} \frac{J_m(\alpha_{mn}^{\pm} r) J_m(\alpha_{mn}^{\pm} r_s)}{Q_{mn}^{\pm} J_m(\alpha_{mn}^{\pm})^2} \mathrm{e}^{-\mathrm{j}\kappa_{mn}^{\pm}(x-x_s)} \right) \quad . \tag{12}$$

Similarly, the expression for an oscillating force dipole in the $x-\theta$ plane is obtained by substitution of

$$\boldsymbol{f}(\boldsymbol{y},\omega) = f_0(\cos\gamma, 0, \sin\gamma)\delta(\boldsymbol{x}-\boldsymbol{y}) \quad , \tag{13}$$

where f_0 is the dipole strength and γ the dipole alignment with the x axis, into Eq. (10) and setting $q(\boldsymbol{y},\omega) = 0$ to yield

$$p(\boldsymbol{x},\omega) = f_0 \sum_{m=-\infty}^{\infty} \mathrm{e}^{-\mathrm{j}m(\theta-\theta_s)} \Bigg(-\frac{1}{2\pi} \sum_{n=1}^{\infty} \frac{J_m(\alpha_{mn}^{\pm} r) J_m(\alpha_{mn}^{\pm} r_s)}{Q_{mn}^{\pm} J_m(\alpha_{mn}^{\pm})^2} \mathrm{e}^{-\mathrm{j}\kappa_{mn}^{\pm}(x-x_s)} \left[\kappa_{mn}^{\pm}\cos\gamma + \frac{m}{r_s}\sin\gamma \right] \Bigg) \quad . \tag{14}$$

The expressions presented in this section for an infinite lined duct containing monopole and/or dipole sources will be referred as 'Green/INF', standing for an analytical Green's function model for an INFinite lined duct.

An infinite number of modes are needed to define the analytical solution given by Eqs.(12-14), and not all of these can be included in practice. Therefore, a parameter to control the series truncation is required. This determines the number of modes included when evaluating the Green's function. This parameter is chosen to be the Cut-Off Ratio (COR). The definition that is often used to define the COR for a mode with radial wavenumber α is [20, 21];

$$\mathrm{COR} = \frac{\alpha\sqrt{1-M^2}}{\omega} \quad . \tag{15}$$

The radial wave number α increases with the mode order. For a given COR all the modes with α smaller than $\frac{\omega \mathrm{COR}}{\sqrt{1-M^2}}$ are therefore included in the modal summation. In a hard-walled duct COR=1 corresponds to the case when only cut-on modes are included. When COR>1 the summation will include a certain number of evanescent modes. The evanescent modes play an important role in the near-field of the source [14] and therefore CORs sensibly higher than unity will often be required in the analysis which follow, since the near field is important when the source is acoustically 'close' the the liner, or indeed in Section 4, close to a mode matching interface.

2.3. In-duct sound power

The non-dimensional acoustic axial power $P(x)$ at each axial cross-section (S) can be used to assess the performance of a liner. It is computed by integrating the intensity field over the duct cross-section [22, 23, 24, 25]. This gives;

$$P(x) = \int_S I_x dS = \frac{1}{2}\int_S \mathrm{Re}\left\{p u_x^* \left(1+M^2\right) + M p p^* + M u_x u_x^*\right\} dS \quad . \tag{16}$$

It is common to analyse the liner acoustic performance using the Sound Power Level (PWL) Insertion Loss (IL), defined as the power relative to the hard-wall case in dB scale, i.e.

$$\mathrm{IL}(x) = 10\log_{10}\frac{P_H(x)}{P_L(x)} \quad [dB] \quad , \tag{17}$$

where P_H and P_L are the acoustic power at a given cross-section for the hard-wall and lined configurations obtained by using Eq. (16).

3. Source power output in hard and lined ducts

In this section, an analysis is presented of the effects that the impedance boundary condition, the source radial position and the excitation frequency have on the acoustic power generated by a monopole and axial dipole point source in infinite hard and lined ducts with and without axial uniform mean flow. Results are presented here for a relatively large number of terms in the modal expansions of expressions (12) and (14) (COR=5 in most cases) The effect of varying COR is discussed in Section 3.3. The axial acoustic power is computed on either side of the source plane by integrating the axial intensity over the cross-section of the duct using Eq. (16). The intensity field is obtained from the Green/INF modal expansions of the pressure and the axial particle velocity. The intensity field is truncated to a finite number of modal contributions and can be integrated analytically. The total power P radiated by the source is obtained by adding the power radiated upstream P^- and downstream P^+, as indicated in Fig. 2.

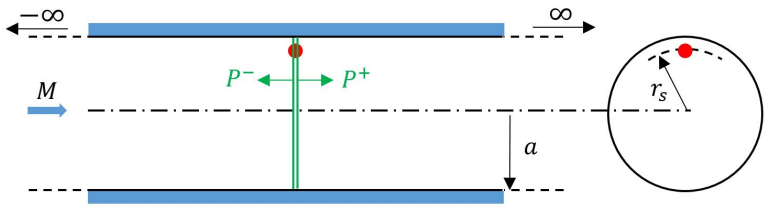

Figure 2: Lateral and cross-section of the infinite circular duct problem and axial acoustic power evaluation *at* the source plane.

Any axial position upstream and downstream of the source gives a unique value for P^- and P^+ in the case of a hard-wall duct because there is no energy loss as the modes propagate axially. However, power must be evaluated in the limit *at* the source plane (as $x \to x_s^-$ and $x \to x_s^+$) for the lined case to exclude any energy dissipated by propagation over the lined walls.

The axial power results presented here are normalised by the power radiated by a monopole or dipole source in free-field. That is, P_d/P_f, the subscripts d and f referring to ducted and free-field respectively. A similar analysis for

monopoles and dipoles has previously been published for a hard-wall duct [26]. It is extended here for lined ducts.

The power output of a monopole source over an infinite plane is also evaluated in this section and compared to the results obtained with the in-duct expressions. The analytical solution of Levine [9] is used for this purpose. The first part of the section deals with a hard-wall duct and the second and third parts deal with a lined duct and the comparison with the half-space problem. The last part combines the hard-wall and lined results to assess the source modification effects in terms of Insertion Loss.

3.1. Source power output in a hard-wall duct

The effects of the source radial position and of the excitation frequency on the normalised power output of the source are plotted in Fig. 3 for the hard-wall case. The horizontal axis represents the normalised distance of the source from the duct centerline. The results indicate that the power approaches the free-field value when the source is located further from the wall and twice this value as it moves closer to the wall. The wall then acts like an image source as demonstrated by the curves approaching a value of 2.0 as $r_s/a \to 1$. The effect of the image source is progressively confined to the vicinity of the wall as the frequency increases. This behaviour occurs both for a monopole (Fig.3a) and a dipole source (Fig.3b) and agrees with the half-plane solutions for all three frequencies plotted as dashed lines.

The results in Fig. 3a are plotted in Fig. 4 in terms of the radial distance from the source to the wall ($e = 1 - r_s$) normalised by the wavelength (λ). Fig. 4a shows the results for a continuous set of source radial locations for a discrete set of frequencies. Conversely, Fig. 4b shows the results for a continuous frequency spectrum for a set of discrete radial source positions. The 'spikes' in the frequency response of Fig. 4b correspond to cut-off frequencies and occur each time a mode cuts on or off. The curves collapse however for different source locations and frequencies, being governed almost entirely by the ratio e/λ. The same qualitative behaviour is evident in both the ducted solution and the half-

space problem and the agreement improves at higher frequencies. Although the normalised results for a dipole are not shown here, the data collapses on the parameter e/λ as for the monopole.

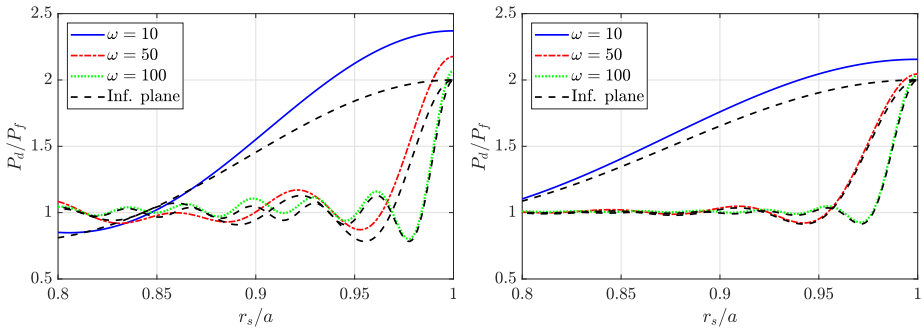

Figure 3: Power generated by a (a) monopole and (b) axial dipole in a hard duct for various radial source positions and excitation frequencies with COR=5 and $M = 0$ and comparison with a half-space equivalent problem [9].

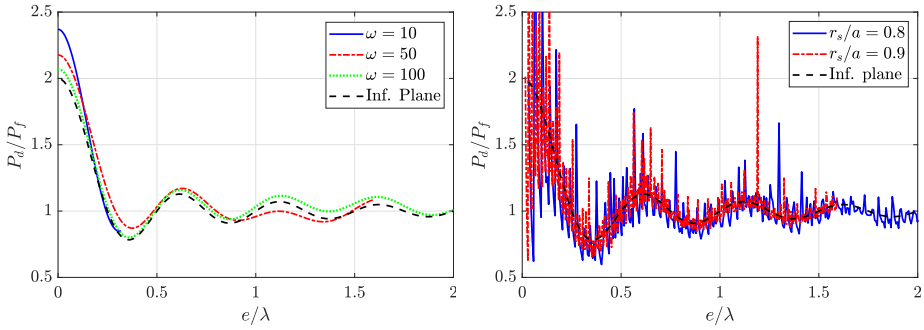

Figure 4: Power generated by a monopole in a hard duct for various normalised radial source positions ($e = 1 - r_s$) and excitation frequencies with COR=5 and $M = 0$ and comparison with a half-space equivalent problem [9].

The total power generated by a monopole and an axial dipole source for various base flow Mach numbers is shown in Fig. 5 plotted against Helmholz number or non-dimensional frequency ($\omega = \tilde{\omega}a/c_0$). These results are compared

to the multi-mode high-frequency Mach number expressions of Joseph et al. [27] relating the dependence of axial sound power with and without flow for an incoherent uniform distribution of sources of arbitrary spatial and temporal order over the duct cross-section. In particular, for the monopole and axial dipole considered in this section;

$$\frac{P^+(M)}{P^+(0)} = \begin{cases} \frac{1}{1+M^2}, & \text{monopole} \\ \frac{3[M^4+M^3-M^2-2M-2(1-M^2)\ln(1+M)]}{M^3(1-M^2)}, & \text{axial dipole} \end{cases} . \tag{18}$$

Note that these expressions are for the acoustic axial power radiated downstream and that to obtain the total power radiated both upstream and downstream one must calculate

$$\frac{P^T(M)}{P^T(0)} = \frac{P^+(+M) + P^+(-M)}{2P^+(0)} . \tag{19}$$

It can be observed in Fig. 5 that the power generated both by a monopole and an axial dipole increases with Mach number. The differences in the peaks observed at lower frequencies are attributed to a different number of modes being cut-on, since the cut-off frequency of each mode changes with Mach number. These trends agree with the high-frequency expressions of Eq. (18), shown in both figures as dashed lines, as the frequency increases

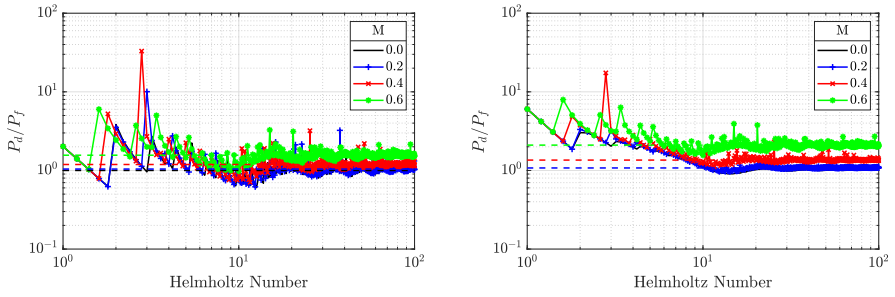

Figure 5: Power spectra of a (a) monopole and (b) axial dipole source for various base flow Mach numbers and $r_s/a = 0.8$. Dashed line: multimode high-ω limit [27].

While the trends in total power radiated by the source for different Mach numbers are similar for the monopole and axial dipole, the proportion of acous-

tic power radiated upstream and downstream varies substantially. The ratio of power radiated downstream and upstream for an axial dipole is shown in Fig. 6. The axial dipole radiates more power upstream than downstream. The monopole radiates exactly the same power upstream and dowstream of the source and hence is not included in Fig. 6. The high-frequency model of [27] can be rearranged to give

$$\frac{P^+(M)}{P^-(M)} = \begin{cases} 1, & \text{monopole} \\ -\frac{M^4+M^3-M^2-2M-2(1-M^2)\ln(1+M)}{M^4-M^3-M^2+2M-2(1-M^2)\ln(1-M)}, & \text{axial dipole} \end{cases} \tag{20}$$

These are shown as dashed lines in Fig. 6 and are in good agreement with the current results.

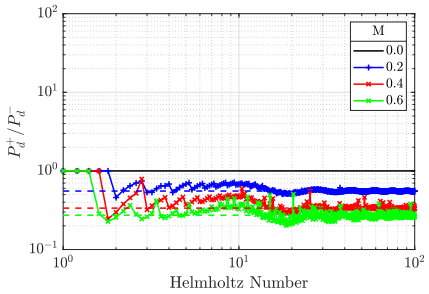

Figure 6: Spectra of the ratio of power radiated downstream and upstream by an axial dipole source for various base flow Mach numbers and $r_s/a = 0.8$. Dashed line: multimode high-ω limit [27].

3.2. Source power output in a lined duct

In this section the analysis of Section 3.1 is applied to lined ducts. Three values of impedance have been used to assess the impact of the liner on the trends observed in Figs. 3-4. The impedance values used are $Z = [1 + \mathrm{j}, 1, 1 - \mathrm{j}]$. The source power is evaluated again on either side of the source plane to characterise the power *generated* by the source before it is attenuated by propagation over the lined surface. Note that the acoustic field at the source plane contains a singularity at the source which is represented in the Green's function solution

by the infinite summation of modes with complex axial wavenumbers. For consistency with the hard-wall case, the number of modes truncated in the infinite mode summation is fixed again by using the hard-wall COR.

The effect of the lined surfaces is demonstrated in Fig. 7, where the results are again plotted in terms of e/λ and the format is the same as for Fig. 4. The trends are similar to those for the hard-wall case in that the results collapse on the non-dimensional e/λ for a significant range of frequencies (ω=10 to 100), and the duct wall has little effect on the source power output provided that the distance between the source and the wall is a significant proportion of one wavelength, this distance depending on the source excitation frequency. As a 'rule of thumb', the source proximity to the wall is only important if the source is located within 1/2 of a wavelength from it. This result holds for all values of impedance tested and is also applicable to a dipole source. However for $e/\lambda < 0.5$ the value of the impedance has a significant impact on the source power output, which can be many times higher than in free-field as e/λ tends to zero. The same behaviour is evident in the half-space equivalent problem. The mechanism by which the source power output increases significantly with its proximity to the wall is further investigated in Section 3.3.

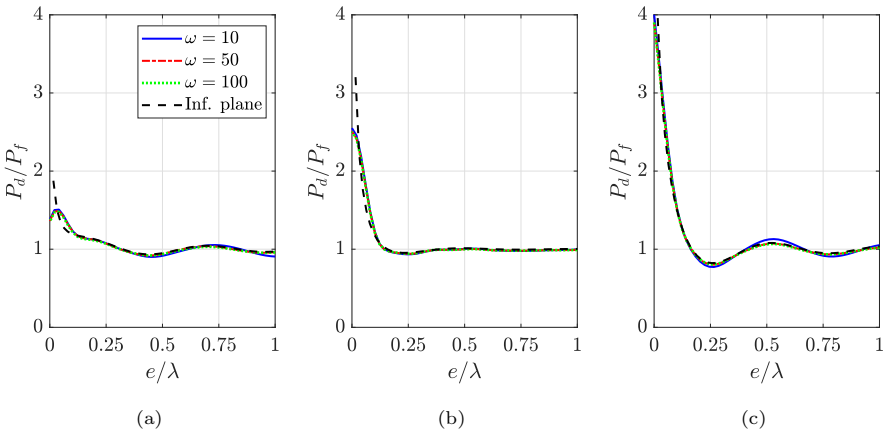

Figure 7: Power generated by a monopole in a lined duct for various impedance values ((a) $Z = 1 + \mathrm{j}$, (b) $Z = 1$ and (c) $Z = 1 - \mathrm{j}$), normalised radial source positions ($e = 1 - r_s$) and excitation frequencies with COR=5 and $M = 0$ and comparison to a half-space equivalent problem [9].

3.3. The effect of the modal truncation parameter (COR) on the solution accuracy

Previous results in this section have been calculated with COR=5. Some aspects of Fig. 4 and Fig. 7 are however sensitive to COR and this is now discussed. The number of modes included in the solution, controlled by the COR, has a significant impact on the predicted power output for source positions acoustically close to the lined wall. This is illustrated in Fig. 8 where the results of Fig. 7 are reproduced for $\omega = 10$, for a range of truncation values for COR. Clearly as the COR increases, the Green's function solutions converge, and approach more closely Levine's result for a half-space problem. These results appear to indicate that both for the infinite half-plane solution, and for the current ducted solution, the source power becomes infinite as $e/\lambda \to 0$. In the ducted case this requires an increasing number of evanescent modes to be included in the truncated Green's function (increasing COR) as $e/\lambda \to 0$. Three values of COR are used in Fig. 8 (COR=1.5, 5 and 10). COR=5 gives converged solutions for $e/\lambda > 0.1$ but higher values are required as e descreases further.

The maximum azimuthal mode order and the total number of modes included in the calculations for ω=10 are listed in Table 2 for each value of COR. Clearly very large numbers of evanescent modes must be included to give converged solutions for very small values of e/λ.

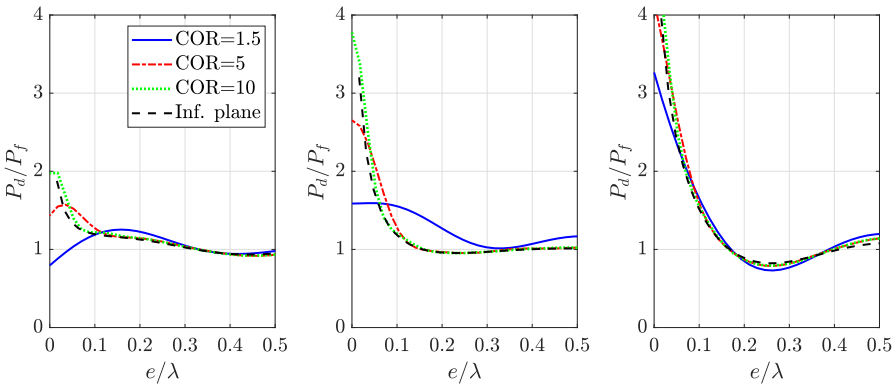

Figure 8: Power generated by a monopole in a lined duct for various impedance values ((a) $Z = 1 + \mathrm{j}$, (b) $Z = 1$ and (c) $Z = 1 - \mathrm{j}$), normalised radial source positions ($e = 1 - r_s$) and CORs with $\omega = 10$ and $M = 0$ and comparison to a half-space equivalent problem [9].

Table 2: Modes included in the solution for $\omega = 10$ and various COR.

COR	$m_{\max}$	N
1	9	17
5	48	333
10	97	1294

The increase in source power illustrated in Fig. 8 as e/λ decreases and the source moves closer to the liner surface appears to contradict experimental evidence that shows a potential *decrease* in acoustic power when the source is close to the liner. This point is now addressed by subdividing the source power output, P_s, into that subsequently absorbed by the lined surface, P_a, and that

radiated to the 'far-field', P_∞. This separation is illustrated in Fig. 9a for the half-space problem and in Fig. 9b for the infinite lined duct. Note that in Fig. 9b the 'far-field' is assumed to lie a finite distance upstream and downstream of the source. Results are presented for the case when this is one half of a duct radius. This is close enough to capture the proximity effects but not so large that the power axial decay is dominant. Levine [9] provides explicit expressions to compute P_s, P_a and P_∞ for the half-space problem. In the ducted case, they are obtained by computing the axial and radial acoustic power across prescribed control surfaces. This decomposition also allows for checking conservation of energy within the control volume, since P_s should equate to $(P_a + P_\infty)$.

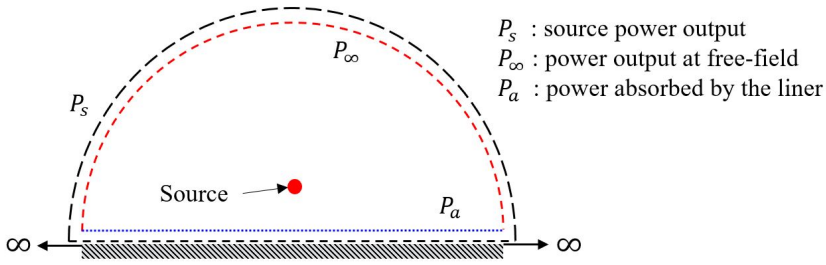

(a)

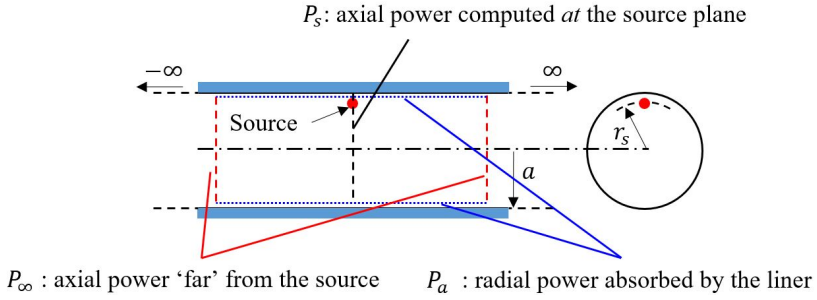

(b)

Figure 9: Decomposition of the source power output P_s into the power observed by the liner P_a and the power radiated to the 'far-field' P_∞ for (a) half-space problem and (b) ducted problem.

The decomposition outlined above is illustrated in Fig. 10 for the ducted and half-space problem. Here the three power components P_s, P_a and P_∞ are

plotted against e/λ. It is observed for both problems that $P_a \to \infty$ for $e/\lambda \to 0$ for all three values of impedance. In contrast, the power radiated to the 'far-field' is finite in all cases and generally *reduces* when the source is located closer to the lined wall. This corresponds to experimental observations in [28, 29, 30]. This data indicates that although the source power increases substantially, due to source modification effects, for sources very close to the liner surface, there is a commensurate increase in the absorption at the liner, with the net result that the sound power radiated to a 'far-field' observer, the red curves in Fig.10, actually decreases as the source approaches the lined surface. This is true both for the half-space solution and for the duct problem.

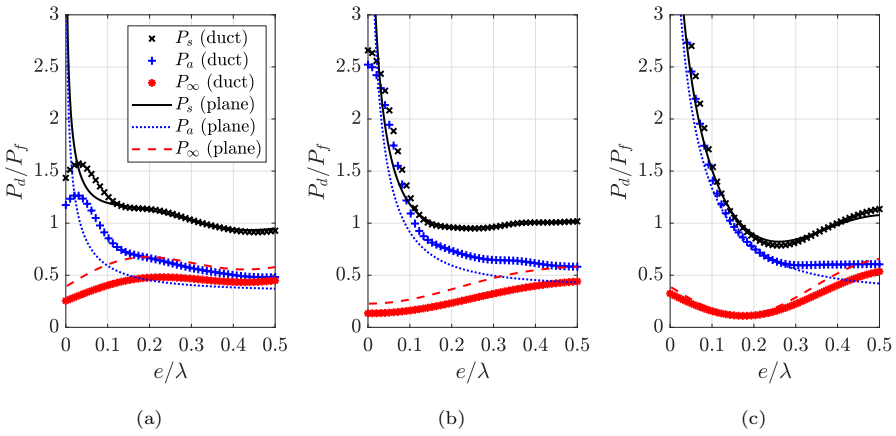

Figure 10: Decomposition of the power generated by a monopole in a lined duct into source power output P_s, absorbed power P_a, and radiated power P_∞ (markers) for various impedance values ((a) $Z = 1 + \mathrm{j}$, (b) $Z = 1$ and (c) $Z = 1 - \mathrm{j}$), plotted against normalised radial source positions ($e = 1 - r_s$) with COR=5, $\omega = 10$ and $M = 0$ and comparison to a half-space equivalent problem [9] (lines).

All results for the lined cases have been presented for $M = 0$. An equivalent decomposition to that in Fig. 10 is shown in Fig. 11 for $M = 0.3$. Trends similar to those in the absence of flow can be observed. Analytical models are not available for the half-space equivalent problem with flow.

The source power modification will vary for each combination of impedance,

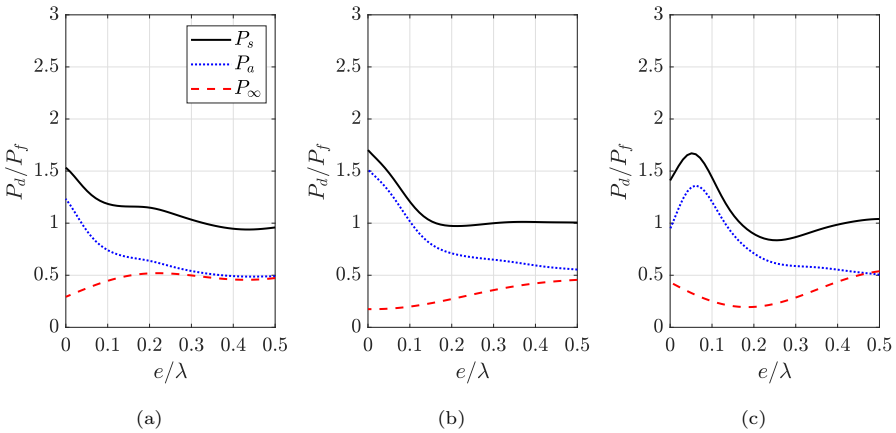

Figure 11: Decomposition of the power generated by a monopole in a lined duct into source power output P_s, absorbed power P_a, and radiated power P_∞ for various impedance values ((a) $Z = 1+\mathrm{j}$, (b) $Z = 1$ and (c) $Z = 1-\mathrm{j}$), plotted against normalised radial source positions ($e = 1 - r_s$) with COR=5, $\omega = 10$ and $M = 0.3$.

source location and source excitation frequency, especially for $e/\lambda < 0.5$. Predictions of power IL therefore involve the effects of the liner attenuation when the sound propagates over the lined surface *and* the variation in the power *generated* by the source due to source proximity effects. This idea is explored in greater detail in the next subsection.

3.4. Implications for PWL Insertion Loss

The source power modifications described in Sections 3.1-3.3 can be applied to estimates of power and power insertion loss specifically for Over-Tip-Rotor liners. To this end, the ducted axial power will no longer be normalised by the source power output in free field but by hard-wall values for the ducted problem.

The axial variation of the absolute PWL for a hard-walled and lined duct is plotted against axial location in Fig. 12 for two radial locations of the source e/λ=[0.1,0.3]. These correspond to r_s/a=[0.94,0.81] respectively. The source is located at $x_s = 0$. The PWL IL at each axial position is obtained, as defined in Eq. (17), as the difference between the hard-walled and lined PWLs. The hard-wall PWL is constant and does not vary in different axial locations since

there is no dissipative process but the lined PWL decays as the waves propagate upstream away from the source due to the liner absorption. It has been observed earlier in this section that the source power output also varies with the wall impedance and frequency. PWL IL can be separated into two contributions as follows

$$\text{PWL IL}(x) = \text{TL}(x) + \Delta\text{PWL}_s = 10\log_{10}\frac{P_L(x_s)}{P_L(x)} + 10\log_{10}\frac{P_H}{P_L(x_s)} \quad , \quad (21)$$

where $\text{TL}(x)$ is the Transmission Loss due to liner *attenuation*, and ΔPWL_s accounts for the variation in the source power *generation* due to the liner impedance, if present, and the back-reaction effects for the lined and hard-wall cases. Note that the hard-wall power (P_H) does not vary with x. This separation of the IL into two components is plotted against axial location from the source in Fig. 12b.

An unusual feature of Fig. 12b is the negative insertion loss for $e/\lambda = 0.3$ at the source plane. This is not inconsistent for this configuration. As discussed previously, the source power output in a hard-wall duct is bounded to twice the free-field power but it can be larger for a lined duct. Hence, close to the source plane, the PWL in a lined duct can exceed, under certain conditions, that in a hard-wall, leading to noise *amplification* (negative IL).

The effect of the source proximity to the wall is characterised by the PWL IL evaluated at the source plane. This provides insight into the noise modification component, and is plotted against e/λ in Fig. 13. The noise modification effects tend to produce a positive IL when the source is acoustically distant from the liner surface (large e/λ) but can lead to up to 3 dB of noise amplification as $e/\lambda \to 0$. For the current value of impedance, it seems that as long as enough liner surface can be acoustically treated, the transmission loss will eventually compensate for a negative ΔPWL_s. However, it may not always be the case for a short lined section, such as in OTR applications, when negative IL can be obtained. This is further discussed in the next section where an analysis is presented for the case when the lined section is of finite length.

The source proximity to the wall has also an impact on the the noise atten-

uation component of Eq. 21 since it determines the modal acoustic excitation in the duct. That is, when the source is close to the wall the mode structure is dominated by high order radial modes that have peak pressure and particle velocity near the wall. This generates local activity close to the wall, which generally correlates with higher noise attenuation.

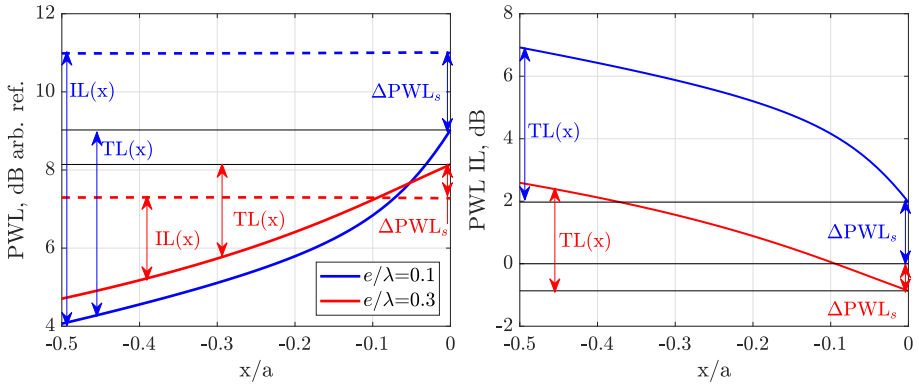

(a) (b)

Figure 12: Axial variation of the PWL and PWL IL for a monopole source located at $x_s/a = 0$ in a lined (solid lines) or hard-wall (dashed lines) duct for $Z = 1 + \mathrm{j}$, COR=5, $\omega = 10$ and $M = 0$.

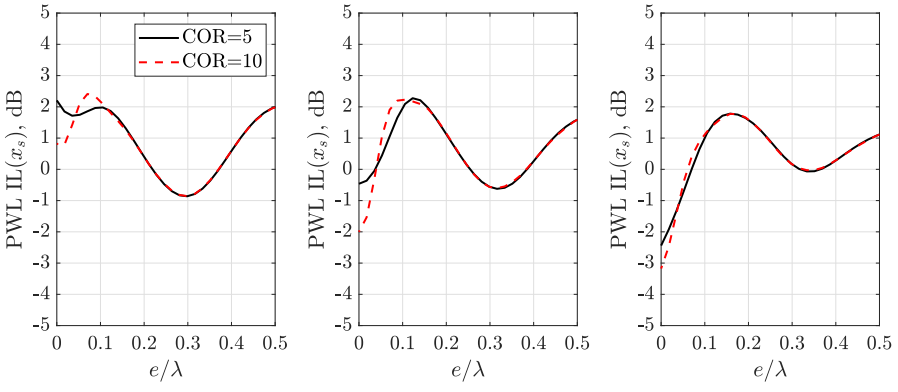

(a) (b) (c)

Figure 13: PWL IL at the source plane for a monopole in a lined duct for various impedance values ((a) $Z = 1 + \mathrm{j}$, (b) $Z = 1$ and (c) $Z = 1 - \mathrm{j}$) and CORs with $\omega = 10$ and $M = 0$.

4. Solution for an infinite duct with a finite length liner (Green/FINF)

The analysis in Section 3 was based on an infinite hard-walled or lined duct. However, in most practical applications the liner is of finite length. An analysis is now presented for this case, that is to say an analytical Green's function is proposed for a Finite length liner connected to INFinite hard-wall extensions. The resulting model will be termed 'Green/FINF'. This model can be used to represent a simple fan stage in which an OTR liner is modelled by a finite lined section. The fan noise is represented by point sources *within* the lined section. A sketch of the problem is shown in Fig. 14. Note that this arrangement can also be extended to model the effect of fancase liners in the absence of an OTR liner by placing the noise sources just downstream of the lined section in the hard-wall semi-infinite duct.

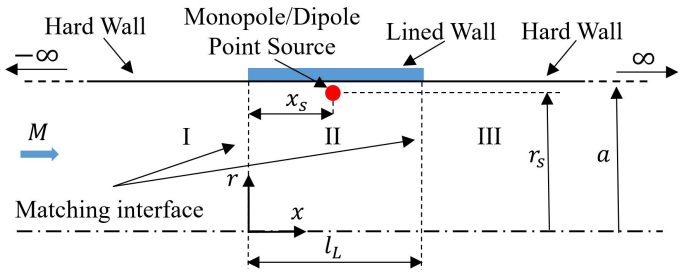

Figure 14: Finite length liner within an infinite hard-wall duct.

A Green's function for this problem is obtained by matching the Green's function of Section 2 to solutions of the homogeneous hard-walled problem at the interfaces between the hard and lined sections. The mode-matching technique is a well-established method for computing the acoustic field in ducts with changes in wall impedance. The traditional approach for mode-mode matching is based on the continuity of acoustic pressure and axial particle velocity on the matching interface. A Galerkin method of weighted residuals is often applied by using the lined or hard-walled eigenfunctions as test functions. This transforms the problem into a set of algebraic equations to determine the modal amplitudes for the combined problem. Detailed descriptions of the method and its applications

are described in the literature [31, 32, 33].

An alternative mode-matching approach formulated by Gabard and Astley [34] is based on the conservation of mass and momentum across the matching interface. Both methods are identical in the absence of mean flow. When axial mean flow is present, however, the second approach results in an additional finite contribution to the matching equations at the matching interface. This improves the accuracy of the solution in the vicinity of the impedance discontinuity when flow is present. More recently, a new mode-matching method was devised by Oppeneer et al. [35] based on closed-form analytical integrals of the modal solutions of the Pridmore-Brown equation allowing for parallel non-uniform shear flow, not relevant for the current work. The traditional mode-matching method and the conservation of mass and momentum approach [34] were both implemented in the current study. Analysis and results are only presented however for the preferred mass and momentum approach.

The novelty of the analysis presented in this section lies in extending the Green's function of Section 2 to include a finite length liner and in presenting the limitations and challenges involved. Mode matching equations are used for this purpose. A similar approach was proposed by Zorumski [12] for a circular duct without flow and a monopole source located on the duct axis, hence considering only axisymetric sound fields.

4.1. The mode-matching method

A single matching interface and the nomenclature to be used are depicted in Fig. 15.

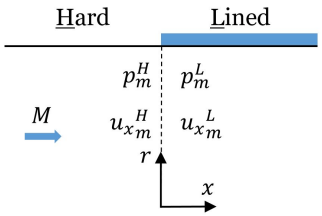

Figure 15: Detail of the matching interface and nomenclature.

The time-harmonic pressure field in a generic cylindrical duct can be expressed as;

$$p(x,r,\theta) = \sum_{m=-\infty}^{\infty} \mathrm{e}^{-\mathrm{j}m\theta} p_m(x,r,\theta) \quad . \tag{22}$$

The impedance of the liner does not vary circumferentially and no scattering occurs between azimuthal modal orders. Therefore, the matching problem can be solved separately for each azimuthal mode number m. Scattering is possible however between radial modes at impedance discontinuities. The pressure field in the hard and lined ducts for each azimuthal order m is given by;

$$p_m^H(x,r,\theta) = \sum_{n=1}^{\infty} \left(A_{mn}^{H+} J_m(\alpha_{mn}^H r) \mathrm{e}^{-\mathrm{j}\kappa_{mn}^{H+} x} + A_{mn}^{H-} J_m(\alpha_{mn}^H r) \mathrm{e}^{-\mathrm{j}\kappa_{mn}^{H-} x} \right) \mathrm{e}^{-\mathrm{j}m\theta} \quad , \tag{23}$$

$$p_m^L(x,r,\theta) = \sum_{n=1}^{\infty} \left(A_{mn}^{L+} J_m(\alpha_{mn}^{L+} r) \mathrm{e}^{-\mathrm{j}\kappa_{mn}^{L+} x} + A_{mn}^{L-} J_m(\alpha_{mn}^{L-} r) \mathrm{e}^{-\mathrm{j}\kappa_{mn}^{L-} x} \right) \mathrm{e}^{-\mathrm{j}m\theta} \quad , \tag{24}$$

expressed as the superposition of right-running (+) and left-running (-) duct modes with coefficients A_{mn}^{+} and A_{mn}^{-} respectively. Note that the radial eigenvalues in the hard section are the same in each direction ($\alpha_{mn}^{H+} = \alpha_{mn}^{H-} = \alpha_{mn}^{H}$).

The corresponding axial particle velocities can be obtained from the pressure field by applying the non-dimensional linearised axial momentum equation. Matching conditions at the hard/lined interface of Fig. 15 will be outlined here for the mass/momentum 'conservation' approach.

In the case of the conservation mode-matching method the non-dimensional corrected matching conditions with uniform mean flow are given by [34]

$$\int_S \overline{W}(p_L - p_H) dS = -\frac{\mathrm{j}M^2}{1-M^2} \frac{1}{\omega} \int_\Gamma \overline{W} \frac{p_L}{Z_L} d\Gamma \quad , \tag{25}$$

$$\int_S \overline{W}(u_{x_L} - u_{x_H}) dS = \frac{\mathrm{j}M}{1-M^2} \frac{1}{\omega} \int_\Gamma \overline{W} \frac{p_L}{Z_L} d\Gamma \quad , \tag{26}$$

where S is the cross-sectional surface of the duct, Γ is its contour and $\overline{W}$ is a weighting function. The terms on the right-hand side represent a finite

contribution from the bounding contour of the matching cross-section. In the traditional pressure/velocity matching approach these terms on the right-hand side are zero, but the additional terms have been shown to improve the accuracy of the mode-matching scheme when compared to reference FE solutions, especially in the vicinity of the impedance discontinuity [34].

Matching equations can be obtained for the conservation matching by substitution of the generic solutions of pressure and axial particle velocity into Eqs. (25-26). The resulting matching equations for each azimuthal mode number m are given by;

$$\int_{r=0}^{1} J_m(\alpha_{mn'}^H r)\left[p_m^L(0,r,\theta) - p_m^H(0,r,\theta)\right] r dr = -\frac{\mathrm{j}M^2}{1-M^2}\frac{1}{\omega} J_m(\alpha_{mn'}^H)\frac{p_m^L(0,1,\theta)}{Z} \quad , \tag{27}$$

$$\int_{r=0}^{1} J_m(\alpha_{mn'}^H r)\left[u_{x_m}^L(0,r,\theta) - u_{x_m}^H(0,r,\theta)\right] r dr = \frac{\mathrm{j}M}{1-M^2}\frac{1}{\omega} J_m(\alpha_{mn'}^H)\frac{p_m^L(0,1,\theta)}{Z} \quad , \tag{28}$$

where $n' = 1$ to N. Eqs. (27-28) then give a set of 2N algebraic equations for the modal coefficients $A_{mn}^{H\pm}$ and $A_{mn}^{L\pm}$. Since the additional terms on the right hand side of Eqs. (27-28) vanish for $M = 0$, the traditional and conservation matching equations are exactly equivalent in the absence of mean flow. The application of the above process and evaluation of the coefficients $A_{mn}^{H\pm}$ and $A_{mn}^{L\pm}$ for the case of a point source in a finite length lined section is given in Section 4.2 to follow.

4.2. Construction of the point source solutions for a finite length liner

The pressure field and particle velocity in each section of Fig. 14 are related by matching conditions at the matching interfaces I-II and II-III. The contribution of the point source can be included in region II by using the superposition principle. It is represented in the first instance by a modal expansion using the sets of known coefficients $A_{mn,s}^{\mathrm{II}\pm}$ obtained by using Green/INF. Note that $A_{mn,s}^{\mathrm{II}-}$ and $A_{mn,s}^{\mathrm{II}+}$ only exist for $0 \leq x \leq x_s$ and $x_s \leq x \leq l_L$ respectively. The corresponding expressions for axial particle velocity are omitted here but can

easily be recovered given that

$$u^{\pm}_{x_{mn}} = \frac{\kappa^{\pm}_{mn}}{\Omega^{\pm}_{mn}} p^{\pm}_{mn} \quad . \tag{29}$$

The Green/INF solution can then be supplemented by any solution of the homogeneous equation and still remain a solution of the inhomogeneous problem in region II, including the point source. This introduces unknown modal coefficients $A^{\mathrm{II}\pm}_{mn}$ into the expressions for pressure and particle velocity in this region. The sound fields in region I and III are simply general solutions of the homogeneous problem for a hard-walled duct. This introduces unknown modal coefficients $A^{\mathrm{I}-}_{mn}$ (region I) and $A^{\mathrm{III}+}_{mn}$ (region III), assuming that both extensions remain anechoic.

When the resulting expressions for p^{I}_m and p^{II}_m are evaluated at the I-II interface we obtain

$$p^{\mathrm{I}}_m(0,r,\theta) = \sum_{n=1}^{N} \left(A^{\mathrm{I}+}_{mn} J_m(\alpha^H_{mn} r) \mathrm{e}^{-\mathrm{j}\kappa^{H+}_{mn} x_a} + A^{\mathrm{I}-}_{mn} J_m(\alpha^H_{mn} r) \right) \mathrm{e}^{-\mathrm{j}m\theta} \quad . \tag{30}$$

$$p^{\mathrm{II}}_m(0,r,\theta) = \sum_{n=1}^{N} \left(A^{\mathrm{II}+}_{mn} J_m(\alpha^{L+}_{mn} r) + J_m(\alpha^{L-}_{mn} r) \left[A^{\mathrm{II}-}_{mn} \mathrm{e}^{+\mathrm{j}\kappa^{L-}_{mn} l_L} + A^{\mathrm{II}-}_{mn,s} \mathrm{e}^{+\mathrm{j}\kappa^{L-}_{mn} x_s} \right] \right) \mathrm{e}^{-\mathrm{j}m\theta} \quad . \tag{31}$$

Similarly at interface II-III ($x = l_L$);

$$p^{\mathrm{II}}_m(l_L,r,\theta) = \sum_{n=1}^{N} \left(J_m(\alpha^{L+}_{mn} r) \left[A^{\mathrm{II}+}_{mn} \mathrm{e}^{-\mathrm{j}\kappa^{L-}_{mn} l_L} + A^{\mathrm{II}+}_{mn,s} \mathrm{e}^{-\mathrm{j}\kappa^{L-}_{mn}(l_L - x_s)} \right] + A^{\mathrm{II}-}_{mn} J_m(\alpha^{L-}_{mn} r) \right) \mathrm{e}^{-\mathrm{j}m\theta} \quad . \tag{32}$$

$$p^{\mathrm{III}}_m(l_L,r,\theta) = \sum_{n=1}^{N} \left(A^{\mathrm{III}+}_{mn} J_m(\alpha^H_{mn} r) + A^{\mathrm{III}-}_{mn} J_m(\alpha^H_{mn} r) \mathrm{e}^{-\mathrm{j}\kappa^{H-}_{mn}(l_L - x_a)} \right) \mathrm{e}^{-\mathrm{j}m\theta} \quad . \tag{33}$$

Substitution of the above expressions into the matching equations (27-28) leads to 2N sets of algebraic equations for the various coefficients A_{mn} at each matching interface, totalling 4N sets of equations:

$$\left[\frac{A^{\mathrm{I}-}_{mn}}{A^{\mathrm{II}+}_{mn}} \right] = T_1 D_1 \left[\frac{A^{\mathrm{II}-}_{mn}}{A^{\mathrm{I}+}_{mn}} \right] + T_{1,s} D_{1,s} \left[\begin{array}{c} A^{\mathrm{II}-}_{mn,s} \end{array} \right] \quad , \tag{34}$$

$$\left[\begin{array}{c} A_{mn}^{\mathrm{III}+} \\ \hline A_{mn}^{\mathrm{II}-} \end{array}\right] = T_2 D_2 \left[\begin{array}{c} A_{mn}^{\mathrm{II}+} \\ \hline A_{mn}^{\mathrm{III}-} \end{array}\right] + T_{2,s} D_{2,s} \left[\begin{array}{c} A_{mn,s}^{\mathrm{II}+} \end{array}\right] \quad , \tag{35}$$

where T_1, T_2, D_1 and D_2 are 2Nx2N transfer matrices. The matrices T_i are square matrices which include analytic integrals of the products of the Bessel functions. The matrices D_i are a diagonal matrices that contain the axial decay rates at the hard and lined duct sections. These equations differ from those used in the absence of sources within the lined section, in the inclusion of the additional terms involving $T_{1,s}$, $T_{2,s}$, $D_{1,s}$ and $D_{2,s}$ on the right hand side of Eqs.(34-35). The coefficients of these matrices are described in detail in Appendix A.

The coefficients defined by the source model ($A_{mn,s}^{\mathrm{II}\pm}$) are known and Eqs.(34-35) can in theory be solved to give the remaining unknown coefficients: $A_{mn}^{\mathrm{I}-}$, $A_{mn}^{\mathrm{III}+}$ and $A_{mn}^{\mathrm{II}\pm}$. Here $A_{mn}^{\mathrm{I}-}$ and $A_{mn}^{\mathrm{III}+}$ correspond to the transmitted modes upstream and downstream into the hard-wall sections, and $A_{mn}^{\mathrm{II}\pm}$, relate to the reflections back into region II at the matching interfaces. Eq. (34-35) can be written as a single system of 4N algebraic equations for the 4N unknown coefficients. In principle these equations can be solved directly but in practice the system is poorly conditioned when a significant number of evanescent modes are included in the modal summations, as is generally the case. A simple iterative scheme such as that outlined in [36] can however be used to generate robust solutions. In this case, the scheme starts by setting $A_{mn}^{\mathrm{II}-}$ initially to zero and computing $A_{mn}^{\mathrm{I}-}$ and $A_{mn}^{\mathrm{II}+}$ by using Eq. (34). Then, $A_{mn}^{\mathrm{II}+}$ is used in Eq. (35) to obtain $A_{mn}^{\mathrm{III}+}$ and a new value of $A_{mn}^{\mathrm{II}-}$. This loop is repeated until the variation of each coefficient with respect to the previous iteration is lower than a specified tolerance δ.

As mentioned previously, an analogous formulation can be adapted to model a fancase liner by placing the point source downstream of the lined section ($x > l_L$). Eq. (34-35) can then be re-written as

$$\left[\begin{array}{c} A_{mn}^{\mathrm{I}-} \\ \hline A_{mn}^{\mathrm{II}+} \end{array}\right] = T_1 D_1 \left[\begin{array}{c} A_{mn}^{\mathrm{II}-} \\ \hline A_{mn}^{\mathrm{I}+} \end{array}\right] \quad , \tag{36}$$

$$\left[\begin{array}{c} A_{mn}^{\mathrm{III}+} \\ \hline A_{mn}^{\mathrm{II}-} \end{array}\right] = T_2 D_2 \left[\begin{array}{c} A_{mn}^{\mathrm{II}+} \\ \hline A_{mn}^{\mathrm{III}-} \end{array}\right] + T_{2,s} D_{2,s} \left[\begin{array}{c} \\ A_{mn,s}^{\mathrm{III}-} \\ \\ \end{array}\right] \quad , \tag{37}$$

where all the matrices are the same except for the source contributions $T_{2,s}$ and $D_{2,s}$ now given as

$$T_{2,s} = \left[\begin{array}{c|c} a & -c^- \\ \hline b^+ & -d^- \end{array}\right]^{-1} \left[\begin{array}{c} -a \\ \hline -b^- \end{array}\right] \quad , \tag{38}$$

$$D_{2,s,ii} = \mathrm{e}^{-\mathrm{j}\kappa_{mi}^{H+}(l_L - x_s)} \quad , \tag{39}$$

where the submatrices a, b, c and d are defined in Appendix A.

Results for finite length liners have been computed by the authors by using the above approach implemented both with the traditional and conservation versions of matching. Both give identical results for zero flow. When flow is present they give results which are very similar to each other except close to the matching interface where small changes are observed. The conservation approach is superior in terms of its underpinning physics and will be used for all the results presented in the remaining part of this section.

4.3. The effect of source proximity to the matching interface

Analytical mode-matching techniques are well established for propagation in ducts with lined sections and simple geometries. In such applications, the 'source' is often approximated by a set of prescribed incident duct modes propagating from an unspecified source upstream or downstream of the lined segment. However, in the current study a modal Green's function representation is used to place the source within the acoustic domain of interest, and indeed to place it close to the liner to allow for source modification. In such configurations additional challenges arise when the source is also located acoustically close to a matching interface. This poses a number of practical issues which are investigated in the current section.

It has been shown in Section 3.2 that an increasing number of evanescent modes are required to capture the back-reaction effects in the power output of a

source as it moves closer to the duct wall. Mode-matching at liner discontinuities must consider at least as many radial terms as those required for the point source representation. The current implementation is controlled by the COR which must be chosen based on the parameter e/λ. The same number of modes is used for mode-matching.

In practice, if the source is located relatively far from the matching plane, the amplitudes of the evanescent modes excited by the source are highly attenuated when evaluated at the impedance discontinuity and have little effect on the matched solution. Conversely, for the case when the source is located close to a matching interface the number of cut-off modes can significantly affect the mode-matching calculations. To illustrate this, the PWL of the field propagating in the upstream hard-wall section (duct section I) is evaluated for a range of source positions within region II, and plotted in Fig. 16 against COR. The non-dimensional length of the OTR liner used for this study is that of the NASA W-8 test rig [7] $l_L = 0.2045$ and the point source is an axial dipole. Solutions are shown for $M = 0$ and $M = 0.3$. In addition to calculations for source positions within the lined section, two additional cases are included where the source is placed close to the interface but downstream of the lined section ($x_s = 1.25 l_L$, fancase liner config.) and well downstream ($x_s = 10 l_L$, a reference case).

It can be observed in Fig. 16 that COR=5 is generally sufficient to give a converged solution (indicated by a horizontal line as COR increases) unless the source is very close to the matching interface. The convergence is faster for the reference case (x_s/l_L=10), where the source is well downstream of the lined section and of the matching planes. The back-reaction effects on the source power caused by the proximity to the impedance discontinuity (matching interface) can be observed by comparing $\mathrm{PWL}^{\mathrm{I}}$ for source positions x_s/l_L=1.25 and x_s/l_L=10. Even though both source locations are in the downstream hard-wall section, the axial power reaching the upstream section can be up to 7 dB lower for the first of these locations closer to the matching plane (see curves for x_s/l_L=[1.25,10] in Fig. 16d), suggesting potential benefits of this configuration.

When the source is located at 1% or 99% of the liner length a converged

solution is not always achieved when flow is present. This limitation is clearly related to the proximity of the source to the nearest matching plane relative to the characteristic wavelength. A value of COR=5 appears however to be sufficient for sources located a distance 0.1λ or more from a matching plane. In practical implementation of the proposed method, it is suggested that the liner be extended artificially a small distance beyond the leading/trailing edge position to avoid this issue.

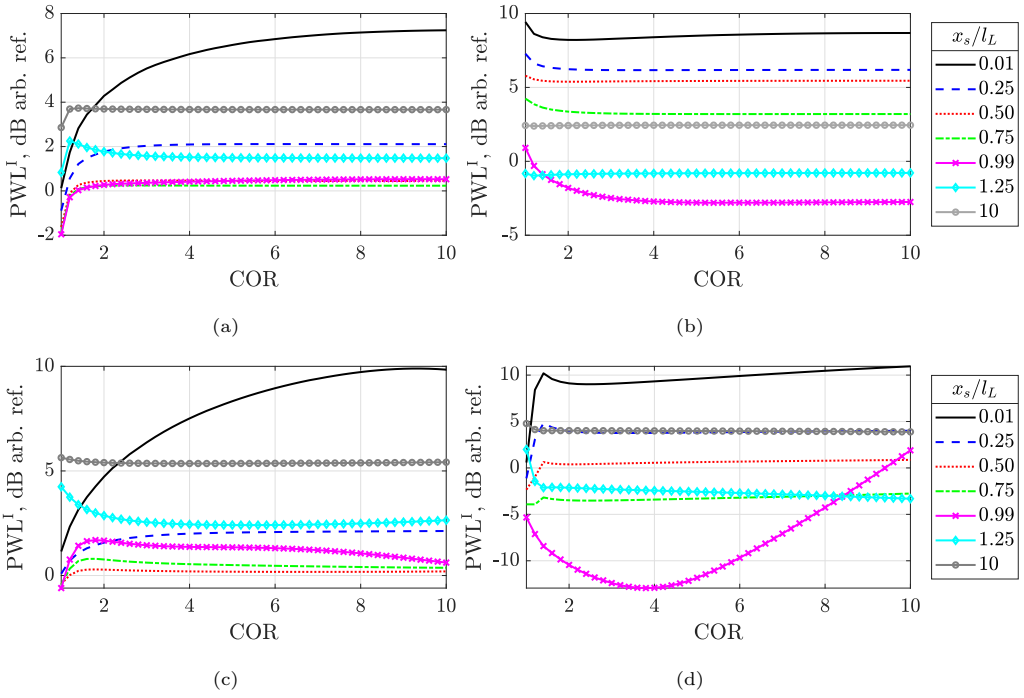

Figure 16: Predicted PWL in the duct section I for ω=15, r_s/a = 0.99, a range of source positions x_s/l_L and CORs. (a) Z=1+j ; M=0.0, (b) Z=1-j ; M=0.0, (c) Z=1+j ; M=0.3, and (d) Z=1-j ; M=0.3.

Clearly the difficulty of obtaining a converged solution when the point source is close to a matching plane, is analogous to that of evaluating the PWL in an infinite lined duct at an axial plane in the near field of the source. All lined modes carry energy, even if they are highly evanescent, leading to a slower convergence rate of the solution closer to the source plane. This reasoning is

illustrated in Fig. 17 where the PWL is plotted along an infinite lined duct for various values of COR for a source located at $x_s = 0$. The asymptotic axial decay is determined by the least attenuated mode. Higher-order predominantly evanescent modes dominate in the near-field and cause slower convergence of the solution with increasing COR when the power is evaluated close to the axial source location. If scattering occurs due to an impedance discontinuity within this region, the effect of the evanescent modes cannot be ignored in matching to the hard-walled extension.

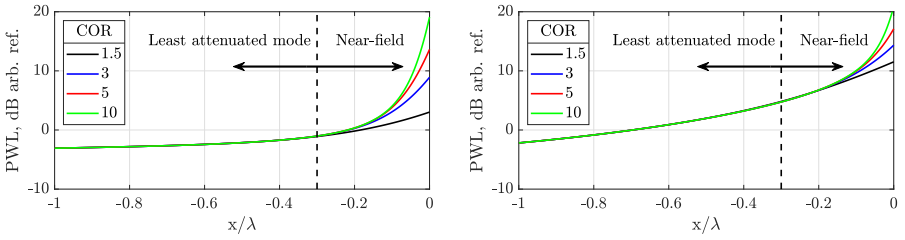

Figure 17: PWL in an infinite lined duct for ω=15, $x_s/a = 0$, $r_s/a = 0.99$, M=0.0, and a range of CORs for (a) Z=1+j and (b) Z=1-j.

The power radiated by a monopole point source in an infinite lined duct (Green/INF) and in a lined duct of finite length (Green/FINF) are now compared. This allows the impact of the finite liner length on the source proximity effects to be assessed. The non-dimensional length of the lined section used here is $l_L = 0.2045$ and the source plane is located at $x_s/l_L = 0.5$. The acoustic power P_d is evaluated in the hard-walled regions I and III for the finite length liner, as shown in Fig. 18a. For a consistent comparison, the acoustic power in the infinite lined duct is evaluated at axial planes located at $x = -0.5l_L$ and $x = +0.5l_L$, as indicated in Fig. 18b. The results are plotted against the normalised radial source location e/λ in Fig. 19. The trends in the source modification effects versus source location are not significantly modified by the impedance discontinuities at the edges of the lined section. Clearly variations due to the reflected modes at the impedance discontinuities are relatively small.

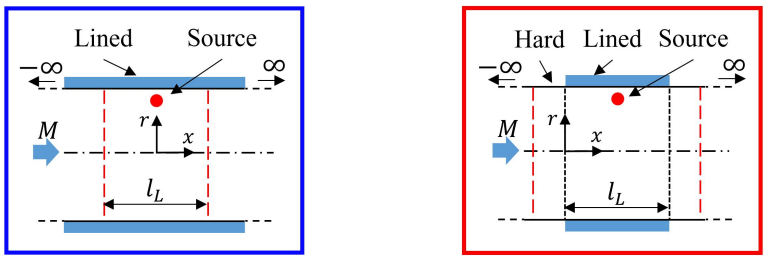

(a) (b)

Figure 18: Evaluation of the acoustic power for (a) Green/INF and (b) Green/FINF used in the comparison of Fig. 19. The evaluation cross-section is indicated by red vertical dashed lines.

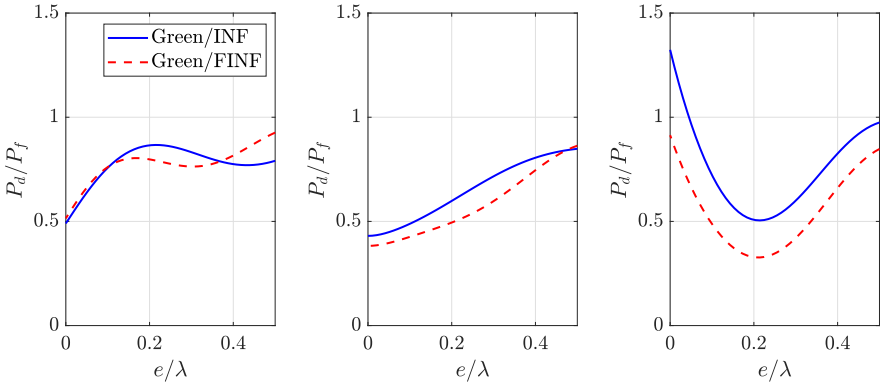

(a) (b) (c)

Figure 19: Radiated power P_∞ predicted with Green/INF and Green/FINF for various impedance values ((a) $Z = 1 + \mathrm{j}$, (b) $Z = 1$ and (c) $Z = 1 - \mathrm{j}$) and normalised radial source positions ($e = 1 - r_s$) with COR=5, $\omega = 10$ and $M = 0$.

4.4. Cross-verification of Green/FINF with FE solutions

Reference FE computations have been performed to cross-verify the analytical solutions obtained with Green/FINF. The numerical simulations have been obtained with the FEM commercial software 'Simcenter 3D Acoustics' with adaptive polynomial order [37]. The domain used for the computations is shown in Fig. 20. It consists of a cylindrical hard-walled duct terminated at each end with a PML-type anechoic boundary condition and with a lined

section, highlighted in orange, which contains a monopole point source. The mesh is refined around the source position ($r_s/a = 0.95$) and at the interface between the hard and lined duct sections.

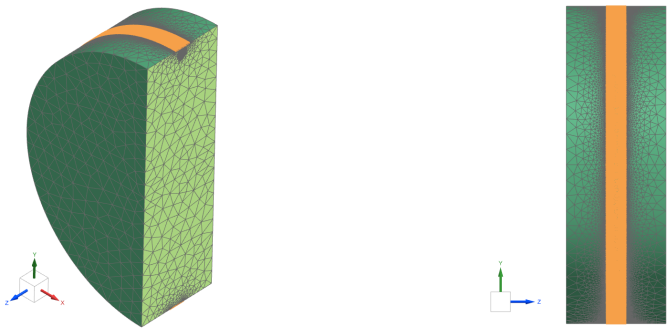

(a) (b)

Figure 20: (a) Isometric view with lateral section and (b) lateral view of the mesh used in the FE simulations for the cross-verification with Green/FINF.

A number of cases have been considered for frequencies ω=[5,10,15], specific acoustic impedances Z=[1+j,1,1-j] and source positions $x_s/l_L = [0.25,0.50,0.75,1.25]$. This test matrix has been repeated for zero mean flow and M=0.3. Results for ω=15 and Z=[1+j,1-j] are presented here but similar agreement has been found in the other cases considered. The conservation matching based on continuity of mass and momentum has been used in the Green/FINF solutions. The analytical and numerical solutions are compared in Fig. 21 in terms of the sound pressure level along the duct wall for the zero flow case. In Fig. 22 results are shown for $M = 0.3$. The vertical thin lines indicate the position of the source plane in each case. In all analytical Green/FINF results presented in this comparison, a COR=5 has been used and provides converged solutions for the data presented here. The analytical and FE solutions are in excellent agreement both with and without flow except in the vicinity of the point source and the matching plane.

Apart from at the matching plane, the most significant discrepancies are in the immediate vicinity of the source, up to 100 % at the source position

itself. This is attributed to the difficulties in evaluating the near-field of the source with the current analytical and numerical approaches. In the analytical solution, the Green/FINF model requires an increasingly higher number of evanescent modes (higher COR) to achieve a converged solution of the sound field in the source near-field region, as illustrated in Fig. 17. In the FE solution, this can be due to the coarseness of the mesh close to the point source when using an adaptive polynomial order solver (FEMAO) based on an *a priori* error indicator. This approach allows the use of a single mesh for a wide range of frequencies and the polynomial order is suitably adjusted for each frequency for an efficient calculation while ensuring a target accuracy. However, the adaptive order does not account well for singular behaviour near the point source and further refinement of the mesh (h-refinement) around the source simply drives down the interpolation order in each element. What is really needed is the inclusion of enriched basis functions in the FE model, not available in standard commercial FE software. However, the integrated effect of the source in the rest of the solution domain is well captured.

In practical applications of the Green/FINF model one is mainly interested in evaluating the sound radiated into the hard-wall sections upstream or downstream of the lined region. Here the agreement with the FE solution is excellent, and a detailed refinement to capture details of the sound field in the 'source' near field region has not been pursued.

Two additional numerical cases have been considered to ensure that multiple sources within the lined section can be modelled accurately by Green/FINF. This has been done by calculating analytically the acoustic field in the duct caused by a number of sources separately and then by superimposing the solutions. The Green/FINF superimposed solutions are compared to FE solutions in which the sources are present simultaneously. The first case comprises 3 sources distributed axially along the lined section at $x_s/l_L = [0.25,0.50,0.75]$. The second case consist of three sources distributed radially for r_s/a=[0.8,0.9,0.99]. The comparisons are shown in Fig. 23 and Fig. 24.

Excellent agreement is achieved between the FE solution with multiple sources

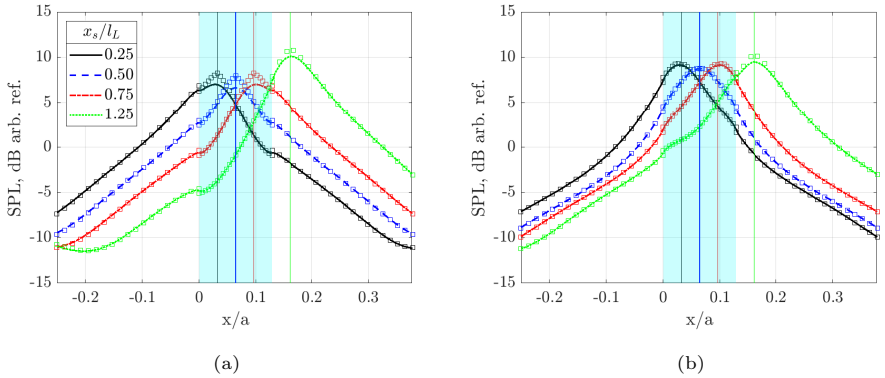

Figure 21: Sound pressure level along the duct wall for ω=15, M=0.0 and COR=5 for (a) Z=1+j and (b) Z=1-j. Lines: FE solution; Squares: Green/FINF solution; Blue-shaded area: lined section.

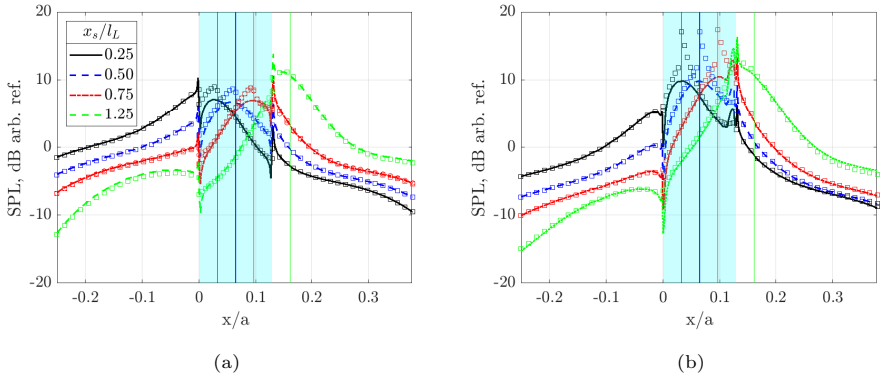

Figure 22: Sound pressure level along the duct wall for ω=15, M=0.3 and COR=5 for (a) Z=1+j and (b) Z=1-j. Lines: FE solution; Squares: Green/FINF solution; Blue-shaded area: lined section.

and the analytical Green/FINF predictions based on the superposition of individual acoustic fields. This comparison provides confidence in applying the Green/FINF model incorporating the mode-matching techniques described here, to cases where more realistic distributed, multiple sources are present in the fan region.

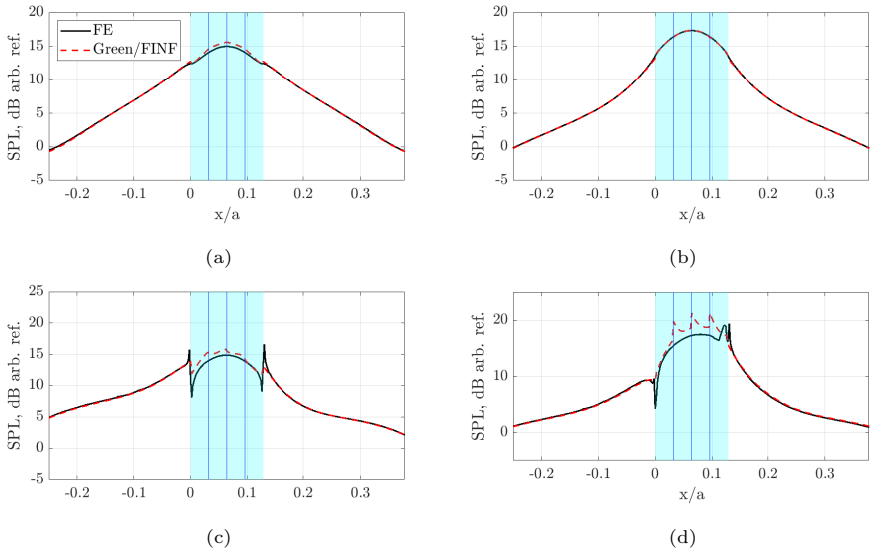

Figure 23: Comparison of the predicted sound pressure level along the duct wall for ω=15 and COR=5 and the FE solution with multiple axial sources. (a) Z=1+j ; M=0.0, (b) Z=1-j ; M=0.0, (c) Z=1+j ; M=0.3, and (d) Z=1-j ; M=0.3. Blue-shaded area: lined section.

5. Conclusions

In this paper two analytical models have been used to predict the acoustic field generated by point monopole and dipole sources in lined ducts with uniform mean flow. The first model, Green/INF, assumes an infinite anechoic lined duct based on an existing Green's function. The second model, Green/FINF, extends the Green/INF Green's function to include a lined section of finite length connected to hard-wall extensions. The connection between the lined segment and the hard-wall extensions is obtained by using mode-matching techniques.

Both models have been used to evaluate the source power output for multiple values of wall impedance, source proximity to the wall, frequency and mean flow Mach number. It has been shown that the PWL Insertion Loss can be divided into two contributions: (1) the noise *attenuation*, measured with the Transmission Loss (TL), and, (2) the *source modification* due to the back-reaction effects for the lined and hard-wall cases. A detailed study of contribution (2) shows

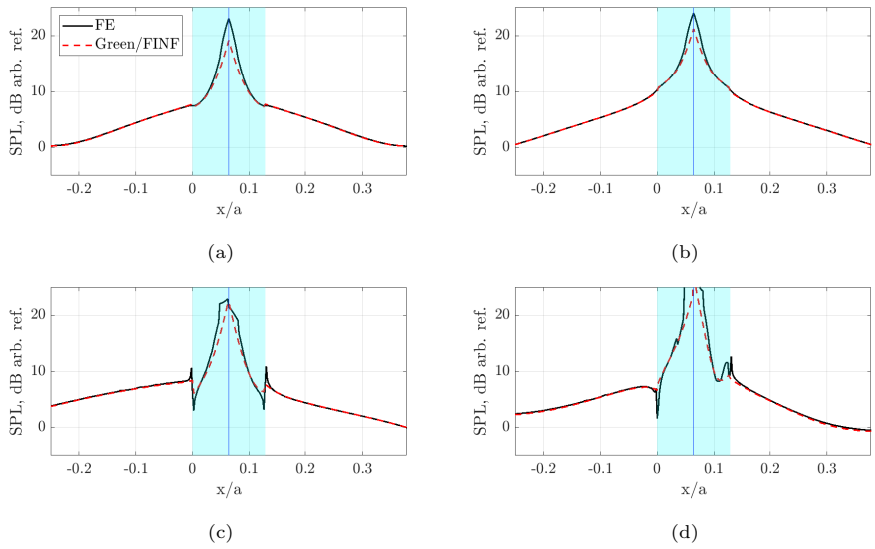

Figure 24: Comparison of the predicted sound pressure level along the duct wall for ω=15 and COR=5 and the FE solution with multiple radial sources. (a) Z=1+j ; M=0.0, (b) Z=1-j ; M=0.0, (c) Z=1+j ; M=0.3, and (d) Z=1-j ; M=0.3. Blue-shaded area: lined section.

that the back-reaction effects become significant when the source is acoustically close to the liner surface ($e/\lambda < 0.5$), in agreement with preliminary experimental data and classical half-space analytical models. A significant number of evanescent modes need to be included in the models to achieve a converged solution when the source is close to the duct wall.

The accuracy of Green/FINF has been demonstrated also by comparison with reference FE solutions and by convergence studies. The application of Green/FINF poses a practical challenge when point sources are located acoustically close to an impedance discontinuity. The effect of evanescent modes is then important and a significant number must be included in the solution. Green/INF and Green/FINF indicate similar trends in predicted source modifications effects. These generally reduce the source power output as the source is located closer to the liner surface.

This work represents the first documented study of radiation from ducted sources (monopole and dipole) which are located very close to acoustically

treated duct walls. The study is prompted by the authors interest in Over-Tip-Rotor (OTR) liners for turbofan aero-engines, for which measured data is now available. The analytic Green's function models demonstrated in the current article provide an analytic tool which can be used in the preliminary design of such liners. The current work indicates however that great care must be taken in using this approach to ensure that a sufficient number of modes are included in the Green's function expansions to ensure that near field evanescent effects, which strongly affect source modification, are correctly modelled. Some guidance is given on how this can be achieved for small values of e/λ where e is the distance of the source from the hard or lined surface and λ is the characteristic wavelength of the source.

The current study is a first attempt at analytic modelling of this problem. Further work is certainly possible which might improve the fidelity of the current results. For example, it is a limitation of the current model that it assumes uniform axial mean flow. While this is a reasonable assumption in the case of OTR liners for turbofan engines, where flow onto the fan is relatively uniform at normal operating conditions, an extension to include the effects of shear flow and of boundary layers could be implemented by using Green's functions based on the Pridmore-Brown equation. The effects of swirl might also be included by use of Green's functions including swirl. These constitute major extensions however and lie well beyond the scope of the current article. The current work would also benefit from a more representative model of the relevant fan rotor sources, including features such as a distribution of dipoles along the fan span, a frequency and spatial dependency of the source strength, possibly based on existing semi-empirical models, or the effects of rotating sources. An extension of the current work including these additional features and a preliminary validation with measured data has been recently presented in [38].

Acknowledgments

This project was funded by the European Union's Horizon 2020 research and innovation programme under a Marie Sklodowska-Curie Innovative Training Network (ITN) grant (Agreement No 722401) within the SmartAnswer consortium. The authors thank Prof. Rienstra for the use of his eigenvalue solver routine, and Dr. Hadrien Beriot for his support in obtaining the numerical solutions using the FE software Simcenter 3D Acoustics.

Appendix A. Mode-matching matrices

The mode-matching matrices are given by

$$T_1 = \left[\begin{array}{c|c} a & -c^+ \\ \hline b^- & -d^+ \end{array}\right]^{-1} \left[\begin{array}{c|c} c^- & -a \\ \hline d^- & -b^+ \end{array}\right] \quad , \tag{A.1}$$

$$T_2 = \left[\begin{array}{c|c} a & -c^- \\ \hline b^+ & -d^- \end{array}\right]^{-1} \left[\begin{array}{c|c} c^+ & -a \\ \hline d^+ & -b^- \end{array}\right] \quad , \tag{A.2}$$

$$T_{1,s} = \left[\begin{array}{c|c} a & -c^+ \\ \hline b^- & -d^+ \end{array}\right]^{-1} \left[\begin{array}{c} c^- \\ \hline d^- \end{array}\right] \quad , \tag{A.3}$$

$$T_{2,s} = \left[\begin{array}{c|c} a & -c^- \\ \hline b^+ & -d^- \end{array}\right]^{-1} \left[\begin{array}{c} c^+ \\ \hline d^+ \end{array}\right] \quad , \tag{A.4}$$

where each element (i, j) of the matrix is defined as

$$a_{ij} = \begin{cases} \displaystyle\int_{r=0}^{1} J_m^2(\alpha_{mi}^H r) r dr & \text{if} \quad i = j \\ 0 & \text{if} \quad i \neq j \end{cases} \quad , \tag{A.5}$$

$$b_{ij}^{\pm} = \begin{cases} \dfrac{\kappa_{mj}^{H\pm}}{\Omega_{mj}^{H\pm}} a_{ij} & \text{if} \quad i = j \\ 0 & \text{if} \quad i \neq j \end{cases} \quad , \tag{A.6}$$

$$c_{ij}^{\pm} = \int_{r=0}^{1} J_m(\alpha_{mi}^H r) J_m(\alpha_{mj}^{L\pm} r) r dr + M\varsigma_{ij}^{\pm} \quad , \tag{A.7}$$

$$d_{ij}^{\pm} = \frac{\kappa_{mj}^{H\pm}}{\Omega_{mj}^{H\pm}} \left[J_m(\alpha_{mi}^{H} r) J_m(\alpha_{mj}^{L\pm} r) r dr \right] - \varsigma_{ij}^{\pm} \quad , \tag{A.8}$$

and

$$D_{1,ii} = \begin{cases} \mathrm{e}^{\mathrm{j}\kappa_{mi}^{L-} l_L} & \text{if} \quad i = 1, ..., N \\ \mathrm{e}^{-\mathrm{j}\kappa_{mi}^{H+} x_a} & \text{if} \quad i = N+1, ..., 2N \end{cases} \quad , \tag{A.9}$$

$$D_{2,ii} = \begin{cases} \mathrm{e}^{-\mathrm{j}\kappa_{mi}^{L+} l_L} & \text{if} \quad i = 1, ..., N \\ \mathrm{e}^{-\mathrm{j}\kappa_{mi}^{H-} (l_L - x_a)} & \text{if} \quad i = N+1, ..., 2N \end{cases} \quad , \tag{A.10}$$

$$D_{1,s,ii} = \mathrm{e}^{\mathrm{j}\kappa_{mi}^{L-} x_s} \quad , \tag{A.11}$$

$$D_{2,s,ii} = \mathrm{e}^{-\mathrm{j}\kappa_{mi}^{L+} (l_L - x_s)} \quad . \tag{A.12}$$

The term $\varsigma_{ij}^{\pm}$ represents the additional contributions one gets by using the continuity of mass and momentum at the matching interface instead of the traditional condition of continuity of pressure and particle velocity. Therefore, this term is zero in the traditional approach and is defined as follows in the conservation approach:

$$\varsigma_{ij}^{\pm} = \frac{jM}{1 - M^2} \frac{1}{\omega Z} J_m(\alpha_{mi}^{H}) J_m(\alpha_{mj}^{L\pm}) \quad . \tag{A.13}$$

The integrals of the products of the Bessel functions can be solved analytically by using [39]:

$$\int_0^a J_m^2(\alpha r_s) r_s dr_s = \frac{1}{2} J_m^2(\alpha a) \left(1 - \frac{m^2}{\alpha^2} \right) \quad , \tag{A.14}$$

$$\int_0^a J_m(\alpha r_s) J_m((\beta r_s) r_s dr_s = \frac{a}{\alpha^2 - \beta^2} \left\{ \beta J_m(\alpha a) J_m'(\beta a) - \alpha J_m'(\alpha a) J_m(\beta a) \right\} \quad . \tag{A.15}$$

References

[1] M. G. Jones, D. Nark, B. Howerton, M. C. Brown, A Review of Acoustic Liner Experimental Characterization at NASA Langley, Tech. Rep. NASA/TP–2020–220583 (2020). doi:10.13140/RG.2.2.15613.10720.

[2] E. Brambley, Review of acoustic liner models with flow, in: Acoustics, 2012.
URL https://hal.archives-ouvertes.fr/hal-00810687/document

[3] R. J. Astley, R. Sugimoto, I. M. Achunche, M. F. Kewin, P. Mustafi, E. P. Deane, A review of CAA for fan duct propagation and radiation, with application to liner optimisation, Procedia Engineering 6 (2010) 143–152. doi:10.1016/j.proeng.2010.09.016.
URL http://dx.doi.org/10.1016/j.proeng.2010.09.016

[4] D. L. Sutliff, D. M. Elliott, M. G. Jones, T. C. Hartley, Attenuation of FJ44 turbofan engine noise with a foam-metal liner installed over-the-rotor, in: 15th AIAA/CEAS Aeroacoustics Conference, no. 3141, 2009. doi:10.2514/6.2009-3141.
URL https://doi.org/10.2514/6.2009-3141

[5] D. L. Sutliff, M. G. Jones, T. C. Hartley, High-Speed Turbofan Noise Reduction Using Foam-Metal Liner Over-the-Rotor, J. Aircraft 50 (5) (2013) 1491–1503. doi:10.2514/1.C032021.
URL http://arc.aiaa.org/doi/10.2514/1.C032021

[6] M. R. Gazella, T. Takakura, D. L. Sutliff, R. Bozak, B. J. Tester, Evaluating the Acoustic Benefits of Over-the-Rotor Acoustic Treatments Installed on the Advanced Noise Control Fan, in: 23rd AIAA/CEAS Aeroacoustics Conference, no. 3872, 2017. doi:10.2514/6.2017-3872.
URL https://doi.org/10.2514/6.2017-3872

[7] R. Bozak, R. P. Dougherty, Measurement of Noise Reduction from Acoustic Casing Treatments Installed Over a Subscale High Bypass Ratio Turbofan Rotor, in: AIAA/CEAS Aeroacoustics Conference, no. 4099, 2018. doi:10.2514/6.2018-4099.
URL https://arc.aiaa.org/doi/10.2514/6.2018-4099

[8] S. Thomasson, Reflection of waves from a point source by an impedance boundary, J. Acoust. Soc. Am. 59 (1976) 780. doi:10.1121/1.380943.
URL https://doi.org/10.1121/1.380943

[9] H. Levine, Output of acoustical sources, J. Acoust. Soc. Am. 67 (6) (1980) 1935–1946. doi:10.1121/1.384459.
URL https://doi.org/10.1121/1.384459

[10] E. J. Brambley, G. Gabard, Reflection of an acoustic line source by an impedance surface with uniform flow, J. Sound Vib. 333 (21) (2014) 5548–5565. doi:10.1016/j.jsv.2014.05.026.
URL http://dx.doi.org/10.1016/j.jsv.2014.05.026

[11] B. J. Tester, C. J. Powles, N. J. Baker, A. J. Kempton, Scattering of sound by liner splices: A kirchhoff model with numerical verification, AIAA J. 44 (9) (2006) 2009–2017. doi:10.2514/1.17678.
URL https://doi.org/10.2514/1.17678

[12] W. E. Zorumski, Acoustic theory of axisymmetric multisectioned ducts, Tech. Rep. NASA-TR-R-419, L-9222 (1974).
URL https://ntrs.nasa.gov/search.jsp?R=19740015161

[13] J. S. Alonso, R. A. Burdisso, Green's functions for the acoustic field in lined ducts with uniform flow, AIAA J. 45 (11) (2007) 2677–2687. doi:10.2514/1.29872.

[14] S. W. Rienstra, B. J. Tester, An analytic Green's function for a lined circular duct containing uniform mean flow, J. Sound Vib. 317 (3-5) (2008) 994–1016. doi:10.1016/j.jsv.2008.03.048.

[15] S. Palleja-Cabre, B. J. Tester, R. J. Astley, R. Bozak, Modelling of Over-The-Rotor Acoustic Treatments for Improved Noise Suppression in Turbofan Engines, in: 25th AIAA/CEAS Aeroacoustics Conference, no. 2580, 2019. doi:10.2514/6.2019-2580.
URL https://doi.org/10.2514/6.2019-2580

[16] B. J. Tester, N. J. Baker, A. J. Kempton, M. C. Wrigth, Validation of an Analytical Model for Scattering by Intake Liner Splices, 10th AIAA/CEAS

Aeroacoustics Conference (2906). doi:10.2514/6.2004-2906.
URL https://doi.org/10.2514/6.2004-2906

[17] B. J. Tester, The propagation and attenuation of sound in lined ducts containing uniform or "plug" flow, J. Sound Vib. 28 (2) (1973) 151–203. doi:10.1016/S0022-460X(73)80102-6.

[18] J. S. Alonso, R. A. Burdisso, Sound Radiation from the Boundary in a Circular Lined Duct with Flow, in: 9th AIAA/CEAS Aeroacoustics Conference and Exhibit, no. 3144, 2003. doi:10.2514/6.2003-3144.
URL https://doi.org/10.2514/6.2003-3144

[19] J. . Alonso, L. Molisani, R. A. Burdisso, Spectral and Wavenumber Approaches to Obtain Green's Functions for Convected Wave Equation, in: 10th AIAA/CEAS Aeroacoustics Conference, no. 2943, 2004. doi:10.2514/6.2004-2943.
URL https://doi.org/10.2514/6.2004-2943

[20] E. J. Rice, Inlet noise suppressor design method based upon the distribution of acoustic power with mode cutoff ratio, Advances in Engineering Science 3 (1976) 883–894.

[21] E. J. Rice, Acoustic liner optimum impedance for spinning modes with mode cut-off ratio as the design criterion, in: 3rd Aeroacoustics Conference, 1976. doi:https://doi.org/10.2514/6.1976-516.
URL https://arc.aiaa.org/doi/abs/10.2514/6.1976-516

[22] C. L. Morfey, Sound transmission and generation in ducts with flow, J. Sound Vib. 14 (1) (1971) 37–55. doi:10.1016/0022-460X(71)90506-2.

[23] C. L. Morfey, Acoustic energy in non-uniform flows, J. Sound Vib. 14 (2) (1971) 159–170. doi:10.1016/0022-460X(71)90381-6.

[24] W. Eversman, Energy flow criteria for acoustic propagation in ducts with flow, J. Acoust. Soc. Am. 49 (1971) 1717. doi:10.1121/1.1912567.

[25] Free Field Technologies, Actran 17.0, Vol. 1.

[26] S. Guerin, A. Moreau, U. Tapken, Relation between source models and acoustic duct modes, in: 15th AIAA/CEAS Aeroacoustics Conference, no. 3364, 2009. doi:10.2514/6.2009-3364.

[27] P. Joseph, C. L. Morfey, C. R. Lowis, Multi-mode sound transmission in ducts with flow, J. Sound Vib. 264 (3) (2003) 523–544. doi:10.1016/S0022-460X(02)01205-1.

[28] S. Palleja-Cabre, B. J. Tester, J. Astley, G. Bampanis, Aeroacoustic assessment of the performance of Over-Tip liners in reducing noise of an aerofoil over a flat surface, in: AIAA AVIATION 2020 FORUM, 2020, pp. 1–21. doi:10.2514/6.2020-2608.
URL https://doi.org/10.2514/6.2020-2608

[29] S. Palleja-Cabre, Fan proximity acoustic treatments for improved noise suppression in turbofan engines, Ph.D. thesis, University of Southampton (2021).
URL http://eprints.soton.ac.uk/id/eprint/450273

[30] S. Palleja-Cabre, B. J. Tester, R. J. Astley, G. Bampanis, Aeroacoustic assessment of the performance of Over-Tip liners in reducing airfoil noise, AIAA J. 59 (9) (2021) 1–30. doi:10.2514/1.J060134.
URL https://doi.org/10.2514/1.J060134

[31] D. L. Lansing, W. E. Zorumski, Effects of wall admittance changes on duct transmission and radiation of sound, J. Sound Vib. 27 (1) (1973) 85–100.

[32] J. F. Unruh, Finite length tuning for low frequency lining design, J. Sound Vib. 45 (1) (1976) 5–14.

[33] A. McAlpine, R. J. Astley, V. J. Hii, N. J. Baker, A. J. Kempton, Acoustic scattering by an axially-segmented turbofan inlet duct liner at supersonic fan speeds, J. Sound Vib. 294 (4) (2006) 780–806. doi:10.1016/j.jsv.2005.12.039.

[34] G. Gabard, R. J. Astley, A computational mode-matching approach for sound propagation in three-dimensional ducts with flow, J. Sound Vib. 315 (4-5) (2008) 1103–1124. doi:10.1016/j.jsv.2008.02.015.

[35] M. Oppeneer, S. W. Rienstra, P. Sijtsma, Efficient mode matching based on closed-form integrals of pridmore-brown modes, AIAA J. 54 (1) (2016) 266–279. doi:10.2514/1.J054167.

[36] A. Cummings, High frequency ray acoustics models for duct silencers, J. Sound Vib. 221 (4) (1999) 681–708. doi:10.1006/jsvi.1999.2030.

[37] Simcenter 3D 2019.2 Documentation (2019).
URL https://docs.plm.automation.siemens.com/data_services/resources/scnastran/2019_2/help/tdoc/en_US/pdf/acoustic.pdf

[38] S. Palleja-Cabre, B. J. Tester, R. J. Astley, Modelling the suppression of rotor-alone fan noise with Over-Tip-Rotor liners and comparison with measurements from a high-bypass turbofan rig, in: AIAA AVIATION FORUM, 2021, pp. 1–19. doi:10.2514/6.2021-2242.
URL https://doi.org/10.2514/6.2021-2242

[39] M. Abramowitz, I. Stegun, Handbook of Mathematical Functions, Dover Publications, INC., New York, 1965.